Biosensors and Bioelectronics 133 (2019) 243–249

Contents lists available at ScienceDirect

Biosensors and Bioelectronics

journal homepage: www.elsevier.com/locate/bios

Two-layer three-dimensional DNA walker with highly integrated entropy-driven and enzyme-powered reactions for HIV detection

Changjing Yuan, Jie Fang, Qiuyue Duan, Qi Yan, Jing Guo, Taixian Yuan, Gang Yi*

Key Laboratory of Clinical Laboratory Diagnostics (Ministry of Education), College of Laboratory Medicine, Chongqing Medical University, Chongqing 400016, China

ARTICLE INFO

Keywords:
Two-layer 3-D DNA walker
Sensor
Entropy-driven reaction
Nb.BbvCI
HIV

ABSTRACT

Here, we propose a new two-layer three-dimensional (3-D) DNA walker sensor with highly integrated entropy-driven and enzyme-powered reactions for the first time. The 3-D DNA walker sensor is constructed by assembling densely carboxyfluorescein-labeled single strand oligonucleotides (inner-layer tracks) and nucleic acid complex S (outer-layer tracks) on a microparticle. In the presence of the target, outer and inner tracks are activated in turn, thereby releasing a great deal of the signal reporters for signal reading. As a result, our 3-D DNA walker sensor can realize the target detection in the range from 2 pM to 5 nM within one hour. Besides, the specific walker sensor can clearly distinguish even one-base mismatched target analogue. More importantly, our walker sensor can also test the target in human serum samples in the concentrations as low as 0.1 nM, which provides a bridge between real sample detection and clinical application. Certainly, this smart strategy could also be generalized to any target of interest by proper design.

1. Introduction

Biological protein-based machines are ubiquitous in living systems, performing various types of physiological functions, including mechanical actuation, intracellular transport, and signal transduction (Schliwa and Woehlke, 2003). Inspired by these biological motors, researchers have attempted to fabricate various artificial molecular machines and motors that can execute specific tasks using controlled molecular-level motion (Qu et al., 2017; Thubagere et al., 2017; Wang et al., 2015). Taking advantages of the predictability, specificity and versatility of Watson-Crick base pairing, various mechanical devices made of DNA molecules have been designed and synthesized, including DNA walkers, DNA tweezers, DNA motors and DNA robots (Liu et al., 2013; Omabegho et al., 2009; Thubagere et al., 2017; Zhou et al., 2015a). In particular, DNA walking devices can be controlled precisely in the programmed oligonucleotide tracks on the micro- or nanoscale and demonstrate great application potential in biological sensing analysis (Jung et al., 2016; Yang et al., 2016).

Currently, the emergence of 3-D DNA tracks has given rise to a new sight of research on DNA walkers. Compared with confined 1-D DNA footpaths (He and Liu, 2010; Liu et al., 2016; Peng et al., 2017; You et al., 2012) or 2-D DNA origami (Tomov et al., 2017; Wang et al., 2017; Yang et al., 2015) as tracks to direct the movement of DNA walkers, 3-D tracks possess more powerful DNA enrichment capacity and better amplification ability (De Luna et al., 2017; Zhang et al., 2018), which is attributed to the large specific surface area of micro- or nanoparticles. For example, Ellington and co-workers have adapted a simple nucleic acid circuit on a microparticle surface through the principle of catalytic hairpin assembly (CHA) for developing the first 3-D DNA walker (Jung et al., 2016, 2017). According to the CHA-based DNA walker, this kind of similar walker appears one after another (Li et al., 2018, 2017; Zheng et al., 2018). Furthermore, Yin and co-workers rationally engineered an elegant entropy-driven DNA walker sensor with 3-D tracks (Liang et al., 2017). In contrast to the CHA-based DNA walkers, entropy-driven DNA walkers employ a sequence of single-stranded linear DNA molecules, which avoids using complicated secondary structures of pseudoknots or kissing loops in DNA molecules, or high background leakage from undesired interactions between metastable hairpin structures. The above enzyme-free 3-D DNA walkers are activated by the purely DNA hybridization reactions.

Despite the high processivity provided by CHA and entropy-driven, 3-D walkers fueled by hybridization are generally of slower kinetics than those fueled by enzymatic cleavages. Undoubtedly, the research of high efficient enzyme-driven 3-D DNA walker has also attracted great attention. Le and his colleagues reported a binding-induced DNA walker with the assistant of nicking endonuclease (Zhang et al., 2015). Such walker sensor demonstrated faster mass transfer than enzyme-free walkers. The whole cleavage of all substrates only required a short time.

* Corresponding author.
E-mail address: yigang666@126.com (G. Yi).

https://doi.org/10.1016/j.bios.2019.03.015
Received 15 December 2018; Received in revised form 2 March 2019; Accepted 8 March 2019
Available online 13 March 2019
0956-5663/

The application of this kind of walker is also reported recently (Feng et al., 2018; Tao et al., 2018). Indeed, each walker sensor has its own unique characteristics due to the principle of unique design. In order to further expand their functionality, it is desirable to develop new 3-D DNA walkers that possess the merits of both intramolecular hybridization and high kinetics. In view of this, the entropy-driven DNA walker and enzyme-powered 3D-DNA walker have attracted our interest.

Acquired immunodeficiency syndrome (AIDS) with high mortality is a common infectious disease caused by the human immune deficiency virus (HIV). The detection of HIV related DNA (HIV DNA) is desirable and important for early diagnosis, therapy of HIV infection and prevention of virus's propagation (Kaushik et al., 2016; Fang et al., 2018). The common methods for clinical diagnosis of HIV infection include enzyme-linked immunosorbent assay (De la Rica and Stevens, 2012), immunofluorescence assay (Pandori et al., 2013) and western blot (Zhou et al., 2015b). Though these methods are accurate, they are unable to identify the “window period” of HIV infection due to the low level of HIV antibody which needs a long period for generating. Polymerase chain reaction (PCR) has evolved as the most frequently used technique for genetic detection because of its high sensitivity and specificity (Ding et al., 2010), but it requires thermal cycling and complicated primer design. Therefore, there is a clear need for researchers to develop simple, rapid and sensitive techniques for the early diagnosis of HIV infection. It is worth noting that the emergence of 3-D DNA walker sensor provides a new method for HIV detection.

In this work, we innovatively design a new two-layer 3-D DNA walker sensor by highly integrated entropy-driven reactions with enzymatic cleavage reactions on microparticles. An entropy-driven intramolecular DNA circular reaction via rational but simple DNA hybridization is designed. When the target exists, the intramolecular hybridization reaction driven by entropy is activated. It enables outer-layer walker portion to achieve automatic walking with concurrent inner-walker chain release. Subsequently, the exposed inner-walker chain is powered by endonucleases to perform autonomously, stepwise movement around the inner-layer 3-D tracks, resulting in the continuous production of the fluorescence signal from rapid enzymatic cleavage of conjugated oligonucleotides. The inner-walker portion of high kinetics for signal release is performed in this step. All above, a novel two-layer 3-D walker sensor is developed for HIV detection in early stage.

2. Experimental

2.1. Reagents and materials

Streptavidin-coated microparticle suspensions (average diameter 1 μm) were purchased from Bangs Laboratory (Fishers, IN). Nb. BbvCI (nicking endonuclease) and 10 × cutsmart buffer were obtained from New England Biolabs (Canada). All oligonucleotides used in this experiment were synthesized by Sangon Biotech Inc. (Shanghai, China) and their detail base sequences were listed in Table S1 respectively. TE buffer (10 mM Tris HCl, 1 mM EDTA, pH 8.0) supplemented with 12.5 mM $MgCl_2$ (TE-Mg^{2+} buffer) was used as the reaction buffer. The oligonucleotides were dissolved in TE-Mg^{2+} buffer and kept at −20 °C. Ammonium persulfate (APS), N,N,N′,N′-tetramethylethylenediamine (TEMED), 30% acrylamide/bis solution and 6 × DNA loading buffer were purchased from Sangon Biotech Inc. (Shanghai, China). 20 bp DNA Ladder (Dye Plus) was from TaKaRa Biotech. GoldView was purchased from Solarbio LIFE SCIENCES (Beijing, China). Ultrapure water obtained from a Millipore water purification system (18.2 MΩ cm, Milli-Q, Millipore) was used in all experiments. All other chemicals were of reagent grade and used as received.

2.2. Apparatus and instruments

Steady-state fluorescence assay measurements were carried out on the Cary Eclipse Fluorescence Spectrophotometer (Agilent, California), using a quartz fluorescence cuvette with an optical path length of 1.0 cm. The excitation wavelength was set at 480 nm with recording emission range of 500–600 nm. Excitation and emission bandwidths were made at 5 nm and 10 nm, respectively. The ultracentrifuge used was Thermo Heraeus Fresco17 (Shanghai, China). The gel electrophoresis was carried out on the DYY-6C electrophoresis analyzer (Liuyi Instrument Company, China) and imaged on a Bio-Rad ChemDoc XRS (Bio-Rad, USA). The characterization of mircoparticles was performed by scanning electron microscope (SEM) (SU8010, Japan).

2.3. Preparation of the 3-D walker sensor

The 3 μL equal volume of Biotin-DW (10 μM) and JA (10 μM) were mixed with 6 μL JB (10 μM) supplied with TE-Mg^{2+} buffer, and the mixture was heated at 95 °C for 5 min in the water bath, followed by slowly decreasing the temperature to room temperature over 5 h. An excess of JB ensured the efficient formation of S (DW/JB/JA) complexes, but did not interfere with the preparation of the 3-D walker sensor. Biotin-SR-FAM was prepared at a concentration of 20 μM in TE-Mg^{2+} buffer, and then mixed with the hybrid compound S in different concentration ratio.

The stock solution of streptavidin-coated microparticles (50 μL) was washed twice with 50 μL binding buffer (20 mM Tris, 1 M NaCl, 1 mM EDTA, pH 7.5, 0.0005% Triton X-100) by centrifuging the microparticles at 10,000 r.p.m. for 3 min, then the supernatant was removed. After resuspending with 50 μL binding buffer, 10 μL different concentration ratio mixture of SR and S was added into the microparticles and incubated for 20 min on a rotator at room temperature. Then, the sample was washed twice with 50 μL TE-Mg^{2+} buffer. Finally, the microparticles through streptavidin-biotin conjugation were suspended with 50 μL TE-Mg^{2+} buffer.

2.4. Detection of HIV DNA by walker sensor

For a typical walker operation on two-layer tracks, a reaction mixture containing 10 μL prepared microparticles, 10 nM JC, varying concentrations of the target and 20 U/100 μL nicking endonucleases in 1 × cutsmart buffer was incubated for 1 h at 37 °C. Following that, the microparticles were allowed to centrifuge at 10,000 r.p.m. for 3 min. After the supernatant was collected, fluorescence signals were measured using a fluorescence spectrophotometer with an excitation/emission wavelength of 480/520 nm.

2.5. Gel electrophoresis

Briefly, 10 μL products of the entropy-driven reaction for 60 min were mixed with 2 μL 6 × DNA loading buffer and analyzed by 12% nondenaturating polyacrylamide gel electrophoresis (PAGE) for 53 min in 1 × TBE buffer (89 mM Tris-boric acid, 2 mM EDTA, pH 8.3) at room temperature under a constant voltage of 120 V. The concentration of different samples in each lane was 200 nM, except 700 nM in lane 5 and lane 7. After electrophoresis, the gel was stained with GoldView at room temperature on a rotator for half an hour. Gel images were analyzed by an UV digital imaging system (Bio-Rad, USA).

2.6. Fluorescence microscope imaging of the walker reaction on the microparticle surface

The slides were cleaned with 75% ethanol and ultrapure water, then sonicated in ultrapure water and dried with N_2. The prepared microparticles that reacted with and without the target were incubated at 37 °C for 1 h followed by washing with TE-Mg^{2+} buffer. 10 μL of the

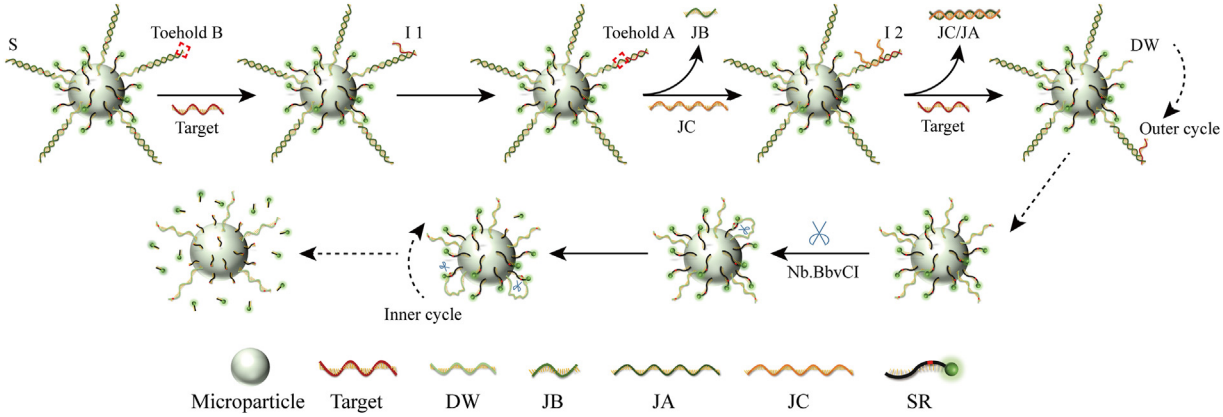

Scheme 1. The principle of amplified analysis of HIV DNA through two-layer 3-D DNA walker sensor.

resulting microparticles were distributed onto the surface of the slides and then imaged using a fluorescence microscope (Nikon 80i, Japan).

3. Results and discussion

3.1. Principle of the two-layer 3-D walker sensor

As shown in Scheme 1, our walker sensor structurally consists of an inner track (M-SR), an outer track (S), fuel (JC) and nicking endonuclease (Nb. BbvCI). HIV DNA acts as both the target and the first-layer walkable leg. The second walker chain bio-DW is designed to be embedded in outer track S. Substrate SR is denoted as a signal reporter, labeled at 3′ end with carboxyfluorescein (FAM), and modified with a biotin at 5′ end to tether to the microparticle surface. There is a 7 nt nicking recognition sequence in the DW, and a 7 nt complementary nicking cleavage sequence in the SR correspondingly. Bio-DW along with JB co-hybridizes to JA and then forms a three-stranded substrate complex S with an overhang at the 5′ end (toehold B). The walker sensor reaction takes place as follows: in the presence of the target DNA, it interacts with JA via single-stranded toehold B on S to form the four-stranded intermediate I1. In this state, the binding between JA and JB is too weak to keep JB attached, leading to the dissociation of JB spontaneously via target toehold-mediated strand displacement and generation of a toehold A on S. Newly exposed toehold A then facilitates the binding of JC, resulting in intermediate I2, which then quickly rearranges to regenerate HIV DNA and release DW by branch migration. Subsequently, the regenerated HIV DNA continues to walk along the outer-layer tracks to trigger autonomous surface-bound S disassembly and concurrent restoration of the initial DW strand. After that, the exposed DW will move inward and hybridize with the complementary sequences of the inner-layer tracks. This hybridization forms a complete recognition sequence of the Nb. BbvCI. The nicking endonuclease-catalyzed cleavage of SR:DW hybrids re-liberates the DW, making it available for hybridization with adjacent SR on the same microparticle. The newly formed double-stranded complex is recognized again by the nicking enzyme so that the walking cycle repeats autonomously along inner-layer tracks. Thus, the two-layer amplifier of 3-D DNA walker sensor is activated in an orderly manner, causing a large amount of SR dispersed into the solution. After centrifugation, the fluorescence of supernatant solutions containing the signal reporters is recorded by the fluorescence spectrophotometer.

3.2. Characterization of the microparticles

First of all, we analyzed the spherical microparticles by SEM. Fig. 1A showed a clear magnification image of the microparticles. The image suggested that the microparticles were uniform in shape and size, and the average diameter of the microparticles was approximately 1 μm. The high quality of microparticles ensured the good performance of our two-layer walker sensor.

3.3. Feasibility of the two-layer 3-D walker sensor

In Fig. 1B, polyacrylamide gel electrophoresis (PAGE) was used to verify outer-layer walker portion of catalytic pathway of entropy-driven reactions. By the reaction of substrate S and fuel JC in the presence of target, the amount of JA/JC produced after 60 min (lane 3) was almost identical to that assessed by annealing the reaction components in lane 1, and the substrate S became shallower than the same amount of lane 2. Besides, there was also a distinct band of DW in lane 3. These results showed that the target could power entropic driving catalytic pathway and dissociate the components of S (Note that Fig. 1C showed how the entropy-driven reaction proceeded). This system behaved as expected: the catalytic reaction of intramolecular hybridization was successful.

To prove the feasibility of inner-layer walker part of the two-layer 3-DNA walker sensor. We examined the fluorescence products from a reaction between M-SR-DW (DW modified M-SR) and 20 U Nb. BbvCI. A control experiment that contained only M-SR-DW was also designed. As seen from Fig. 1D, the slight fluorescence increase was observed in the control experiment due to the residual unconjugated SR dissolved in the suspension. However, the obvious fluorescence intensity can only be recorded in the presence of Nb. BbvCI. The results suggested that Nb. BbvCI played a specific and significant role in promoting the quick release of FAM-labeled SR payloads, verifying the success of inner-layer walker portion design.

We next examined our two-layer walker sensor with the target DNA. As Fig. 2A illustrated, weak fluorescence signal was found when no target existed, while a rapid increase in fluorescence was observed in the presence of the target and the signal-to-noise ratio reached 9.63. Based on these results, we might make a preliminary conclusion that our design of two-layer walker sensor could be used for the detection of the target DNA.

Moreover, in order to visually validate that the walker sensor was activated by the HIV DNA, the fluorescence microscope was also used to analyze the feasibility of the walker sensor. As expected, when no target was incubated in the reaction system, a large amount of green fluorescent was randomly distributed in the field of sight (Fig. 2B). Arrows indicated regions where green fluorescence showed the location of the fluorescein-modified microparticles. However, after walker was initiated by adding target DNA, few green microparticles were observed (Fig. 2C), indicating that the target successfully started the two-layer walker reaction on the surface of microparticles. The above results confirmed our smart and autonomous two-layer walker sensor was completely feasible for HIV nucleic acid detection.

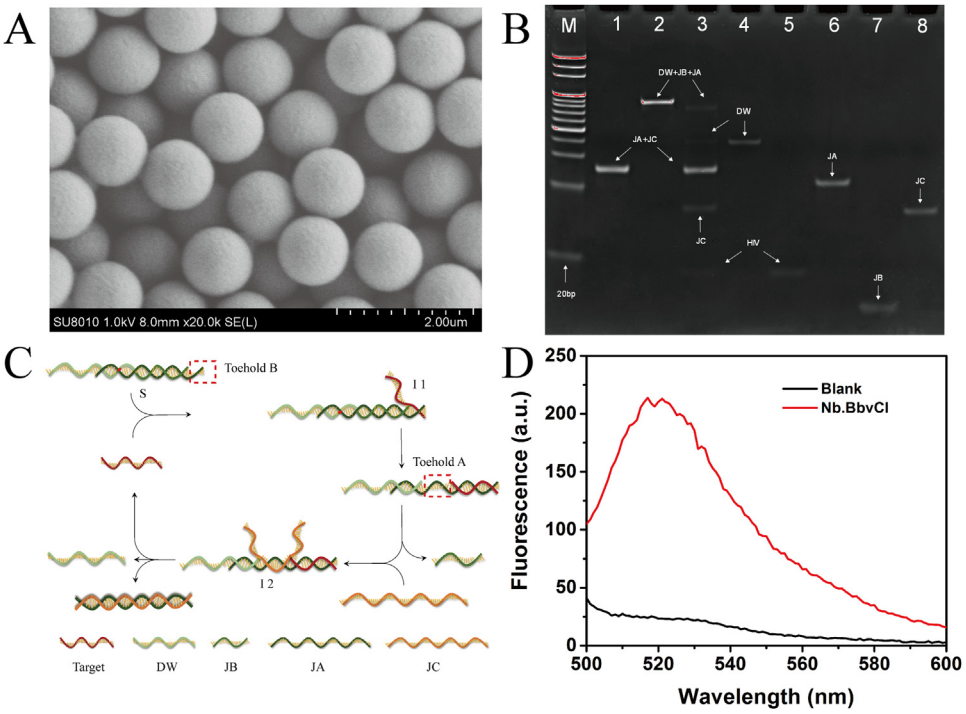

Fig. 1. (A) SEM images of microparticles. (B) Verification of the entropic driving catalytic pathway by the PAGE (12% native gel). All reactions are run at 25 °C for 53 min. Line M is 20 bp DNA marker. Line 1, the reaction substrate JA + JC. Line 2, the reaction component of DW + JB + JA. Line 3, the products of DW/JB/JA in the presence of HIV and JC. Line 4, DW. Line 5, HIV. Line 6, JA. Line 7, JB. Line 8, JC. (C) The principle of outer-layer walker part of entropy-driven reaction. (D) The significant role of Nb.BbvCI in our walker sensor. Fluorescence intensity of the inner-layer of walker sensor in the absence and presence of Nb.BbvCI at the same concentration of HIV, respectively.

3.4. Optimization of experimental conditions

To make an optimal analytical performance of our two-layer walker sensor, the number of bases in toehold B, the ratio of SR and S, the hybridization time and the concentration of Nb. BbvCI were optimized in detail by using 5 nM HIV DNA as a model.

It is vital to improve the rate of toehold-mediated strand exchange for the outer-layer walker on the surface of microparticles. We designed a series of toehold B with different base length to find the best one. As seen in Fig. 3A, with the base length of toehold B increasing, the walker sensor was easier to start, and the fluorescence intensity was also enhanced accordingly. When the base length of toehold B exceeded 9, the signal dropped sharply. Furthermore, at the condition of toehold 8, the best signal-to-noise ratio was 13.35 (Fig. 3B), so it was doubtless that toehold 8 was used in all subsequent experiments. The phenomenon of decreasing fluorescence may be due to the so strong binding between HIV DNA and JA that multiple cycles of target HIV cannot be achieved.

The coverage ratio of SR and S was another key factor, because SR was both signal reporter and the cleavable substrate on the microparticles, which can potentially affect the property of the DNA walker sensor. To clarify the effect of the coverage ratio between SR and S, the concentration of SR was set as 2000 nM and the S was varied from 40 to 200 nM. As presented in Fig. 3C, intuitively, the increased coverage of S resulted in a higher fluorescence signal until the ratio of SR and S was 20:1. However, the further increase of S decreased the fluorescence intensity. This probably because of the charge repulsion and steric hindrance between the high-density S on the same microparticle. Thus, we determined the satisfied ratio of SR and S was 20:1.

Besides, the time curves from the operation of the walker sensor (Fig. 3D) illustrated that the fluorescence signal intensity increased with prolonged reaction time. However, the fluorescence signal-to-noise ratio (Fig. 3E) reached a plateau at 60 min. As for the efficient reaction time, it may be attributed to the fact that target can trigger the DW while the DW can release many signal reporters. At the same time, the inner-layer design made DW hold itself in persistent on microparticle surface and prevented it from dissociating into the buffer, so that DW could contact with the SR efficiently. On the other hand, the increase in local effective concentrations of SR also accelerated

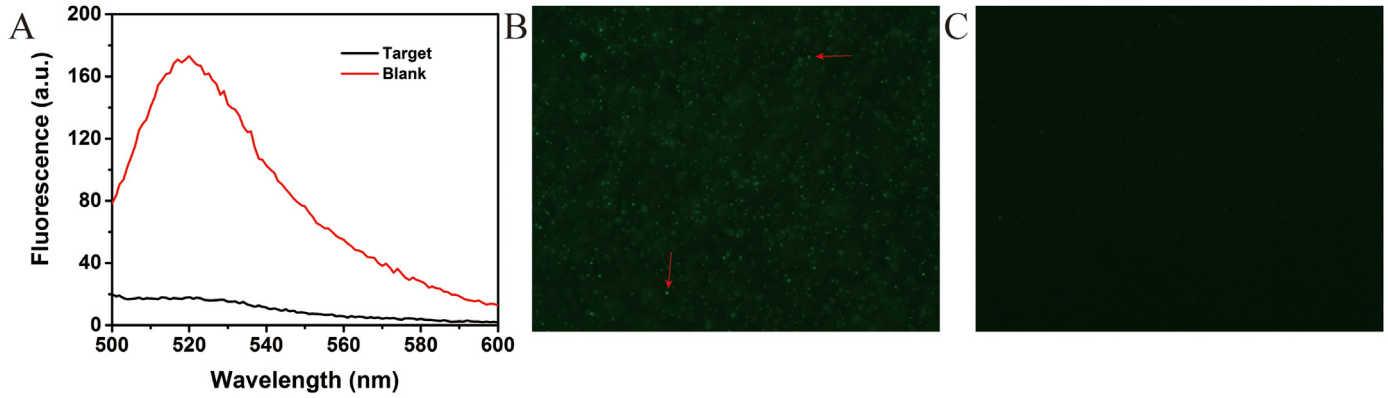

Fig. 2. (A) Fluorescence signals responses corresponding to the feasibility of our two-layer walker sensor. The peak curve and flat curve are the analysis of the 5 nM HIV and 0 nM HIV. All experimental conditions are the same. (B) Fluorescence micrograph showing a lawn of fluorescein-modified microparticles. Arrows indicated regions where microparticles took on green fluorescence. (C) A micrograph of the result when target initiates the reaction of the two-layer walker on the microparticle surface.

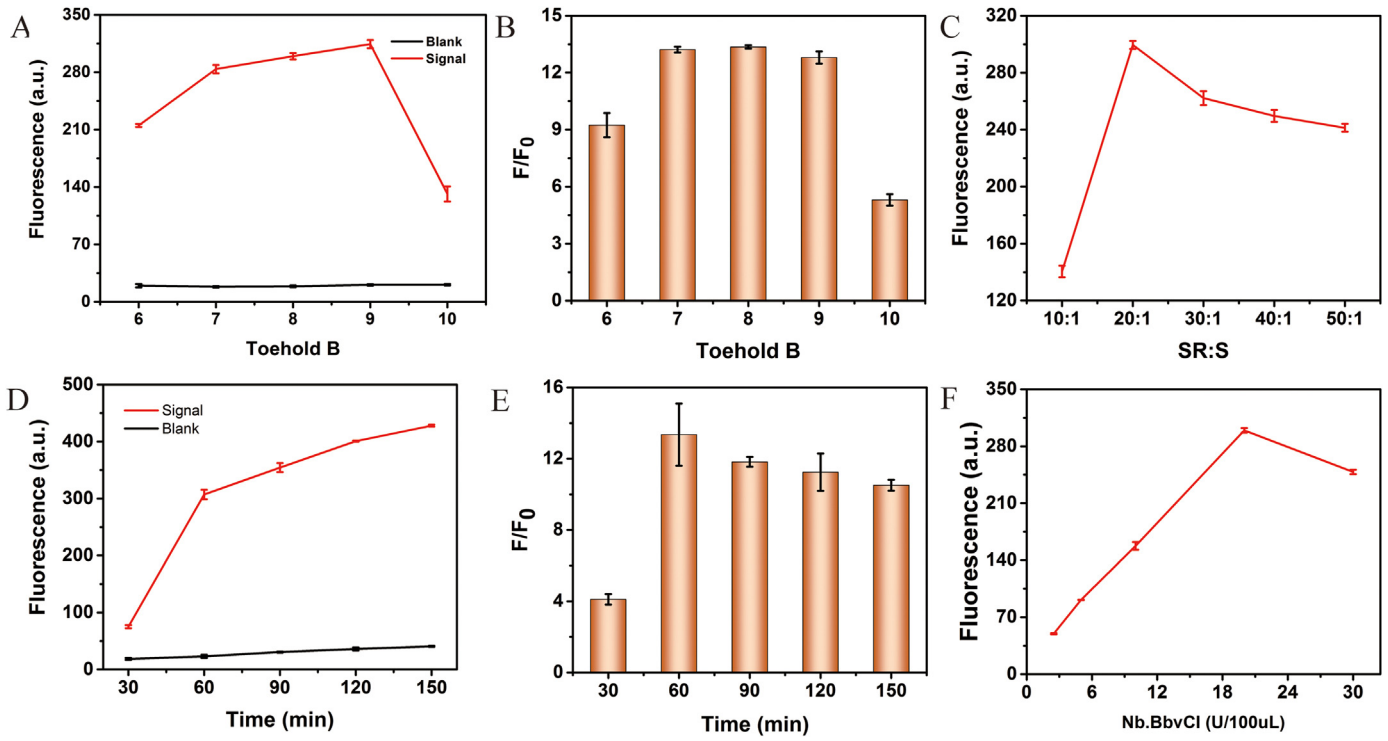

Fig. 3. (A) Effect of toehold B length on the signal values triggered by 5 nM HIV. (B) Signal-to-noise ratio of different toehold B length in the presence of 5 nM HIV DNA. (C) Optimization of the ratio between SR and S. (D) Changes of fluorescence values related to different incubation time of our two-layer walker sensor according to the Scheme 1. All conditions of experiments are the same except hybridization time. (E) Signal-to-noise ratio of different reaction time in the presence of 5 nM HIV DNA. (F) The dosage of nicking nuclease. Error bars indicate one standard deviation of triplicated test.

enzymatic cleavage, making the 3-D DNA walker sensor amenable for the task of rapid payload release.

As Nb. BbvCI was a critical component of the walker sensor, the performance of the walker sensor was tested at different concentration of Nb. BbvCI. As shown in Fig. 3F, the fluorescence signal of the walker sensor was significantly enhanced by improving the concentration of the nicking endonuclease up to 20 U/100 μL. However, when the concentration of the enzyme was further increased, the fluorescence signal leveled off. This result indicated that 20 U/100 μL Nb. BbvCI was sufficient enough to power walker sensor. Consequently, 20 U/100 μL nicking endonuclease was chosen to ensure the good performance of our walker sensor.

3.5. Analytical performance of the 3D-DNA walker sensor

Upon construction of the DNA walker sensor on the basis of the optimal experimental condition, we then investigated its analytical performance for quantifying the target DNA. As expected, the fluorescence signal gradually increased with the increase in concentrations of the target DNA. By plotting the fluorescence intensity versus target concentration (Fig. 4A), we can detect the target DNA across 2 orders of magnitude from 2 pM to 5 nM (Fig. 4B). The regression equation was expressed as $FI = 25.00709 + 0.05507 \times C_{target}$, with a correlation coefficient R^2 of 0.99985. Compared with other reported methods, our proposed 3-D DNA walker sensor had prior analysis capability (Table S2). Apparently, the superior analysis capability can be attributed to the following three aspects. Firstly, high efficient intramolecular multiple turnover target became a vital factor in increasing sensitivity. Secondly, the specific nicking nuclease with high kinetics could rapidly cleave the abundant signal indicator to obtain the signal amplification. Thirdly, the conjugation of two-layer DNA components on the same microparticle can greatly increase their local effective concentrations, thus enhancing the sensitivity of the walker sensor.

To assess the usability and dependability of the developed method in complicated biological environment, we also challenged our walker sensor for detecting the target in human serum samples. Taking laboratory biosafety into consideration, samples from AIDS patients had not been used. Our walker sensor was conducted by spiking varying concentrations of target DNA in human serum samples. In Fig. 4C, it was noticeable that fluorescence signal were detected in human serum. The obtained regression equation was expressed as $FI = 46.51269 + 0.05342 \times C_{target}$, with a correlation coefficient R^2 of 0.94343 and the actual detection limit was 100 pM Furthermore, real-time fluorescent quantitative PCR (qPCR) was introduced to verify the quantitative accuracy. The plots of the cycle thresholds (Ct) vs. the logarithm of target DNA concentration showed a strong linear relationship in the range from 50 pM to 1 nM, with the correlation coefficient of 0.99766 (Fig. S1A). When comparing the results of two assays using regression analysis, the plots of Ct obtained with the qPCR assay vs. that of fluorescence signals obtained with the established two-layer 3-D DNA walker biosensor give a R^2 value of 0.98779 (Fig. S1B), confirming the satisfactory consistency of two methods. These results indicated the potential applicability of our proposed walker sensor for HIV DNA detection in real biological samples.

In the principle of walker sensor application, it needs to meet three aspects of requirements: high specificity, acceptable reproducibility and good stability. Our 3-D DNA walker sensor was also high specificity in identifying the target DNA, estimated by the four kinds of DNA sequences, including the target DNA (T), single-base mismatched DNA (M1-1, M1–2, M1–3), two-base mismatched DNA (M2) and three-base mismatched DNA (M3) at the same concentration. Fig. 4D showed a good fluorescence signal output and the best specificity in response to T. In addition, the response of T was about 2 times, 5.6 times, 9 times, 15.3 times, 15.6 times as that of M1-1, M1–2, M1–3 M2 and M3 respectively. Our walker sensor was able to differentiate the target from target analogues which even contained only one mismatched base. This was probably due to the fact that toehold induced entropy-driving reactions promote the ability of two-layer 3-D DNA walker sensors to

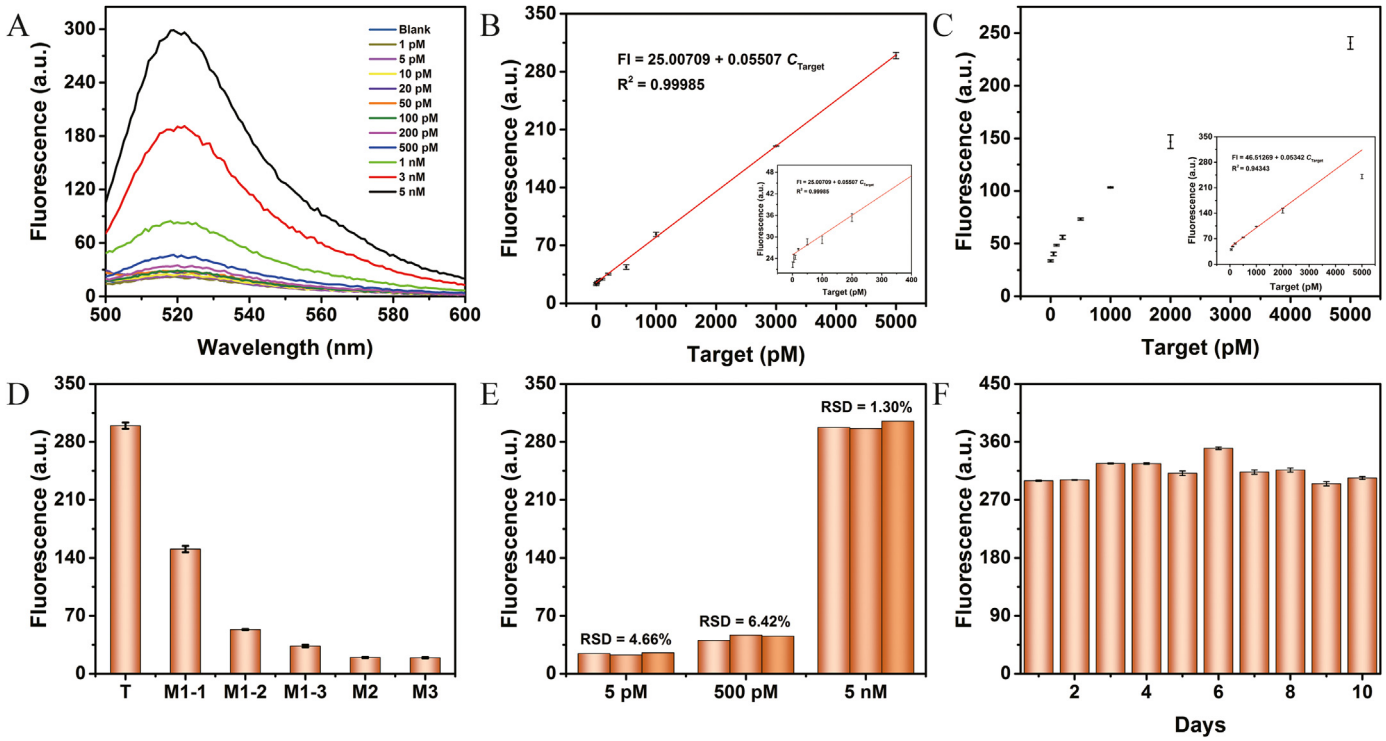

Fig. 4. (A) Fluorescence spectrum of the two-layer 3-D DNA walker sensor with target HIV of different concentrations in cutsmart buffer: 0, 1, 5, 10, 20, 50, 100, 200, 500, 1000, 3000, 5000 pM (B) Ploting the fluorescence intensities verse target concentration ranging from 1 pM to 5 nM. Inset shows the linear response at low concentrations from 1 pM to 200 pM (C) Fluorescence scatter plot of the two-layer 3-D DNA walker sensor with target HIV of different concentrations in human serum sample: 0, 50, 100, 200, 500, 1000, 2000, 5000 pM. Inset shows the calibration curve of the walker sensor for target from 100 pM to 2000 pM (D) Specificity of two-layer 3-D DNA walker sensor against different kinds of target analogues. Fluorescence intensities in response to the target, the single-base mismatch, two-base mismatch and three-base mismatch of target. (E) Reproducibility of the proposed walker sensor among three times detection in different concentration of target samples. (F) Stability of the proposed walker sensor during 10 days storage at 4 °C. Error bars indicate one standard deviation of triplicated test.

distinguish DNA sequences with single nucleotide variations. The reproducibility of the strategy was examined by three repetitive experiments with 5 pM, 500 pM and 5 nM HIV DNA respectively. As can be seen from the Fig. 4E, relative standard deviation (RSD) of three different concentration of HIV DNA was 4.66%, 6.42% and 1.30% respectively. The data suggested that the proposed walker sensor had well reproducibility. Furthermore, the stability of this walker sensor during storage at 4 °C for consecutive 10 days was also confirmed by the target detection with the walker sensor. It is clear from the Fig. 4F that no apparent loss in activity of our walker sensor was observed. The RSD of 10 days period tests was 0.68%, revealing the good stability of walker sensor during long-term storage.

4. Conclusions

Unlike the reported 3-D DNA walkers that are single-layer orbitals, our ingenious two-layer walker runs on double-layer tracks. The smart two-layer 3-D DNA walker sensor with high sensitivity and efficiency is successfully used for HIV DNA detection at picomolar level in one hour. Meanwhile, the proposed walker sensor shows high specificity toward the HIV DNA even with single nucleotide variations. Also, our walker sensor testes the target in undiluted human serum samples and obtains a good linear relationship. In a word, the concept of integrating two reactions on a single particle has made it easier to expand the functionality of 3-D DNA walkers. The new strategy may lead to the development of novel DNA walkers and devices for bioanalytical applications.

Acknowledgements

This work was supported by the Science and Technology Research Program of Chongqing Yuzhong District Science and Technology Commission (Grant No. 20180127) and the Special Fund Project Key Laboratory of Clinical Laboratory Diagnostics (Ministry of Education).

Credit author statement

Changjing Yuan involved in the design, execution of the work and wrote the first draft of the manuscript. Jie Fang contributed on concept, and interpretation. Qiuyue Duan, Qi Yan, Jing Guo and Taixian Yuan provided advice and assisted in reviewing the original draft. Dr. Gang Yi supervised the work.

Declaration of competing interests

none

Appendix A. Supporting information

Supplementary data associated with this article can be found in the online version at doi:10.1016/j.bios.2019.03.015.

References

De la Rica, R., Stevens, M.M., 2012. Nat. Nanotechnol. 7 (12), 821–824.
De Luna, P., Mahshid, S.S., Das, J., Luan, B., Sargent, E.H., Kelley, S.O., Zhou, R., 2017. Nano Lett. 17 (2), 1289–1295.
Ding, G.C., Heuer, H., Zuhlke, S., Spiteller, M., Pronk, G.J., Heister, K., Kogel-Knabner, I., Smalla, K., 2010. Appl. Environ. Microbiol. 76 (14), 4765–4771.
Fang, B.Y., Li, C., An, J., Zhao, S.D., Zhuang, Z.Y., Zhao, Y.D., Zhang, Y.X., 2018. Nanoscale 10 (12), 5532–5538.
Feng, C., Wang, Z., Chen, T., Chen, X., Mao, D., Zhao, J., Li, G., 2018. Anal. Chem. 90 (4), 2810–2815.
He, Y., Liu, D.R., 2010. Nat. Nanotechnol. 5 (11), 778–782.

Jung, C., Allen, P.B., Ellington, A.D., 2016. Nat. Nanotechnol. 11 (2), 157–163.
Jung, C., Allen, P.B., Ellington, A.D., 2017. ACS Nano 11 (8), 8047–8054.
Kaushik, A., Vabbina, P.K., Atluri, V., Shah, P., Vashist, A., Jayant, R.D., Yandart, A., Nair, M., 2016. Biosens. Bioelectron. 86, 426–431.
Li, N., Du, M., Liu, Y., Ji, X., He, Z., 2018. ACS Sens. 3 (7), 1283–1290.
Li, N., Zheng, J., Li, C., Wang, X., Ji, X., He, Z., 2017. Chem. Commun. 53 (60), 8486–8488.
Liang, C.P., Ma, P.Q., Liu, H., Guo, X., Yin, B.C., Ye, B.C., 2017. Angew. Chem. Int. Ed. 56 (31), 9077–9081.
Liu, M., Cheng, J., Tee, S.R., Sreelatha, S., Loh, I.Y., Wang, Z., 2016. ACS Nano 10 (6), 5882–5890.
Liu, M., Fu, J., Hejesen, C., Yang, Y., Woodbury, N.W., Gothelf, K., Liu, Y., Yan, H., 2013. Nat. Commun. 4, 2127.
Omabegho, T., Sha, R., Seeman, N.C., 2009. Science 324 (5923), 67–71.
Pandori, M.W., Westheimer, E., Gay, C., Moss, N., Fu, J., Hightow-Weidman, L.B., Craw, J., Hall, L., Giancotti, F.R., Mak, M.L., Madayag, C., Tsoi, B., Louie, B., Patel, P., Owen, S.M., Peters, P.J., 2013. J. Clin. Virol. 58 (Suppl 1), e92–e96.
Peng, L., Zhang, P., Chai, Y., Yuan, R., 2017. Anal. Chem. 89 (9), 5036–5042.
Qu, X., Zhu, D., Yao, G., Su, S., Chao, J., Liu, H., Zuo, X., Wang, L., Shi, J., Wang, L., Huang, W., Pei, H., Fan, C., 2017. Angew. Chem. Int. Ed. 56 (7), 1855–1858.
Schliwa, M., Woehlke, G., 2003. Nature 422 (6933), 759–765.
Tao, F., Fang, J., Guo, Y., Tao, Y., Han, X., Hu, Y., Wang, J., Li, L., Jian, Y., Xie, G., 2018. Anal. Biochem. 554, 16–22.
Thubagere, A.J., Li, W., Johnson, R.F., Chen, Z., Doroudi, S., Lee, Y.L., Izatt, G., Wittman, S., Srinivas, N., Woods, D., Winfree, E., Qian, L., 2017. Science 357 (6356).
Tomov, T.E., Tsukanov, R., Glick, Y., Berger, Y., Liber, M., Avrahami, D., Gerber, D., Nir, E., 2017. ACS Nano 11 (4), 4002–4008.
Wang, D., Vietz, C., Schroder, T., Acuna, G., Lalkens, B., Tinnefeld, P., 2017. Nano Lett. 17 (9), 5368–5374.
Wang, L., Deng, R., Li, J., 2015. Chem. Sci. 6 (12), 6777–6782.
Yang, X., Tang, Y., Mason, S.D., Chen, J., Li, F., 2016. ACS Nano 10 (2), 2324–2330.
Yang, Y., Goetzfried, M.A., Hidaka, K., You, M., Tan, W., Sugiyama, H., Endo, M., 2015. Nano Lett. 15 (10), 6672–6676.
You, M., Chen, Y., Zhang, X., Liu, H., Wang, R., Wang, K., Williams, K.R., Tan, W., 2012. Angew. Chem. Int. Ed. 51 (10), 2457–2460.
Zhang, H., Lai, M., Zuehlke, A., Peng, H., Li, X.F., Le, X.C., 2015. Angew. Chem. Int. Ed. 54 (48), 14326–14330.
Zhang, P., Jiang, J., Yuan, R., Zhuo, Y., Chai, Y., 2018. J. Am. Chem. Soc. 140 (30), 9361–9364.
Zheng, J., Li, N., Li, C., Wang, X., Liu, Y., Mao, G., Ji, X., He, Z., 2018. Biosens. Bioelectron. 107, 40–46.
Zhou, C., Duan, X., Liu, N., 2015a. Nat. Commun. 6, 8102.
Zhou, L., Huang, J., Yu, B., Liu, Y., You, T., 2015b. ACS Appl. Mater. Interfaces 7 (44), 24438–24445.